Computer simulation of ion-exchange membrane electrodialysis for salt concentration and reduction of RO discharged brine for salt production and marine environment conservation

Yoshinobu Tanaka[a*], Monica Reig[b], Sandra Casas[b,d], Carlos Aladjem[c], Jose Luis Cortina[b,d]

a IEM Research, 1-46-3 Kamiya, Ushiku-shi, Ibaraki 300-1216, Japan

b Chemical Engineering Dept. UPC-Barcelona TECH, Av. Diagonal 647, 08028 Barcelona, Spain

c SOLVAY Iberica SL. C/Marie Curie 1-3-5, 08760 Martorell, Spain

d CETAQUA Carretera d'Esplugues, 75, 08940 Comella de Llobregat, Spain

* Corresponding author, Tel.: +81-29-874-5400, E-mail address: fwis1202@mb.infoweb.ne.jp

ABSTRACT

The salt discharged from reverse osmosis (RO) is concentrated by ion-exchange membrane electrodialysis (ED) to produce salt for industrial use while the salt concentration is reduced to seawater level in order to prevent environmental impact on marine ecosystems. The technology was evaluated experimentally and discussed with a computer simulation program of the ED system incorporated with U-shape cells. The algorithm computes mass transport, energy consumption, electric current leakage, concentrate NaCl purity, pressure drop and limiting current density. The sea water RO discharged brine was supplied to the ED pilot plant and it was operated changing current density and temperature taking benefit of seasoning variations.

The computed energy consumption E_{NaCl} and NaCl concentration in concentrated solutions C''_{NaCl} are compared to the experimentally observed values. The correlation coefficients are $R(r)$ = 0.863 for E_{NaCl} and $R(r)$ = 0.553 for C''_{NaCl}. Thus the reasonability of the developed algorithms is supported by the experiments. The current leakage is nearly three percent for any electric current. The pump driving force is ca. $1 - 2$ percent of energy consumption. The limiting current density is very high (over ten times of current density). In order to decrease salt concentration at the outlets of desalting cells to seawater level, it is necessary to increase desalting ratio to 0.5. This technique however increases E_{NaCl} and decreases C''_{NaCl}. In spite of this operating circumstance, E_{NaCl} and C''_{NaCl} are comparable to the data in the salt manufacturing plant operation to produce edible salt. NaCl produced from the RO discharged brine ED is competitive in the edible salt market.

1. Introduction

The 21st century is called "the century of water" because of the water crisis due to the population increase and environmental destruction. The fresh water from surface water (rivers and lakes) and ground water totals only 0.01 % of total water resources on the earth. To secure adequate water resources, effective and cyclic utilization of water are available, but at the same time, desalination of seawater which accounts for 97.54 % of total water resources is realistic. Seawater desalination is carried out extensively at present particularly in the Arabian Gulf, Mediterranean Sea, Red Sea, Southeast Asia, etc. The main desalination processes are multi-stage flash distillation (MSF), multiple-effect distillation (MED) and reverse osmosis (RO). In order to produce clean drinking water, the seawater environment is expected to be clean. However, it is a contradiction that the effluent and emission produced by the desalination plants are affecting the seawater environment.

Seawater desalination plants produce drinking water and discharge concentrated brine which has a higher density than seawater. The brine spreads over the sea floor in shallows, so it is usually dissipated by a diffuser system to be mixed with seawater [1]. However, the perfect mixing of a large amount of the discharged brine with surrounding seawater is impossible. In a closed water area such as Arabian Gulf, Mediterranean Sea etc., the discharged brine increases seawater concentration and pollutes seawater because it dissolves several chemical additives, chemical cleaning solutions and pretreatment chemicals [2 − 6]. It impairs marine life and induces negative environmental impacts such as diminishing the biological diversity [7 - 10]. We have to pay attention further to the fact that desalination plants require significant amounts of thermal and electrical energy, which causes greenhouse gas emissions and global warming [11]. Pérez-González et al. [12] gave an overview on the treatments to overcome the environmental problems associated to the direct discharge of RO concentrates. Xu et al. [13] reviewed strategies and technologies for concentrate management, including disposal, treatment, and beneficial use.

The process described in this article is the RO-ED hybrid system, which has been also postulated in similar investigations. Thomas [14] reported zero discharge seawater desalination, integrating the production of freshwater, salt, magnesium and bromine. The process used ED to reduce the salinity of the reject stream from RO so that the salt-depleted rejection stream could be recycled to the RO to improve the yield of freshwater. Zhang et al. [15] investigated the feasibility of ED on the RO concentrate to reduce the volume of salty water discharged and to

improve the overall water recovery to produce infiltration water for groundwater recharge. In the pilot system, the decarbonation process was used to reduce scaling potential of the feed or the concentrate stream of the ED. Tran et al. [16] investigated the feasibility of a hybrid system consisting of a pellet reactor and ED to treat RO concentrate in which the pellet reactor was used to remove the scaling potential before ED treatment. The objective of the hybrid system was a high recovery for the RO system, and zero liquid discharge for the RO. McGoven et al. [17] discussed RO-ED hybrid system by modeling the energy and equipment costs of ED as a function of product salinity. Specifying the feed salinity along with the product salinity and flow rate, the equations were solved using a non-linear equation solver to compute the final concentrate concentration, total membrane area, energy consumption, specific equipment cost, specific energy cost, and specific water costs. Tanaka et al. [18] discussed operating parameters of an ion-exchange membrane electrodialytic salt manufacturing plant using brine discharged from a RO seawater desalination plant. The energy consumption in the salt manufacturing process using RO discharged brine was 80 % of the consumption in the process using seawater. Casas et al. [19] studied a technology to concentrate NaCl from RO reject in order to be reused in the chlor-alkali industry. A mathematical model was developed based on the Nernst-Planck equations to predict the performance of the ED pilot plant. The model was able to accurately predict the NaCl concentration reached, time required to reach maximum concentration and production overflow as a function of the operation conditions. Reig et al. [20] concentrated NaCl from seawater RO brines for chlor-alkali industry by the ED pilot plant, and discussed the limiting current density, the behavior of miner and trace species dissolving in the brine and energy consumption. Jiang et al. [21] electrodialyzed highly concentrated brine from RO plant to produce coarse salt and freshwater, and investigated the effect of operation parameters such as current density, operation mode, type of membranes and initial brine concentration.

This article discusses the technology of salt concentration and reduction of RO discharged brine by ion-exchange membrane (IEM) electrodialysis (ED) for salt production and marine environment conservation. The investigation is carried out at first to develop the computer simulation program describing the performance of the ED system. Next, real RO discharged brine is supplied to the pilot plant and it is operated changing current density and temperature. The computed energy consumption and NaCl concentration in concentrated solutions are compared to the observed values. Computer simulation is one of the useful tools to discuss the performance of electrodialyzers and widely applied to the technology development [22 - 29].

The previous work (Reference [18]) includes the original concept of the computer program, but it is impossible to calculate the performance of electrodialyzers. The other previous works (References [19, 20]) extended experimental observation vigorously, but quantitative analysis is insufficient. The current investigation successfully discusses the experimental results using the

computer program updated in the succeeding investigation [30]. The computer simulation program is now accessible through a companion website, and it provides a guideline for designing, manufacturing and operating practical-scale electrodialyzers [31].

2. Electrodialysis process

In Fig. 1, RO discharged brine (Feeding solution, salt concentration C'_{in}) is supplied to desalting cells (inlet linear velocity; u'_{in}), partition cells and electrode cells. The concentrated solution is circulated between concentrating cells (inlet linear velocity; u''_{in}) and circulation tank and an electric current I is passed through electrodes. Salt concentration in concentrating cells and in the circulation tank is increased with time and reaches to a steady state. After C'' (salt concentration in concentrating cells) and C'_{out} (salt concentration at the outlets of desalting cells) reach steady values, C'' and C'_{out} are measured.

Structure of the flow-pass in the cell is classified to an I-shape and a U-shape. Flow-pass structure in the ED pilot plant described in this article is incorporated with U-shape cells (Photo 1). The computer simulation program is applicable to the I-shape cell as illustrated in Fig. 2. Thus it is necessary to create an imaginary I-shape cell equivalent to a U-shape cell. In this investigation, the structure of the imaginary I-shaped cell is assumed to be illustrated by Fig. 2. Fig. 3 shows the structure of a spacer integrated in desalting and concentrating cells.

Fig. 4 illustrates the mass transport in an imaginary I- shape cell pair in an electrodialyzer operating in a steady state with a constant electric current I. A salt solution (raw salt solution, concentration: C'_{in}) is supplied to the inlets of desalting cells (De) at average linear velocity of $u'_{in.}$ A concentrated solution (concentration: C'') is supplied to the inlets of concentrating cells (Con) at the inlet average linear velocity of u''_{in}. Ions and solutions transfer from a desalting cell to a concentrating cell across an IEM pair and their flux is defined by J_S and J_V respectively.

3. Electrodialysis program

The performance of the ED unit operating in a steady state can be computed with a single computation in the spreadsheet using a common software (Excel) and ordinary hardware (computer). Fig. 5 shows the ED program chart. It is operated by inputting the source code *i.e.* optional process specifications and operating conditions of the unit integrated with imaginary I-shaped cells. The program consists of the equations explained below:

3.1 Membrane characteristics

Ion flux J_S and solution flux J_V transported from desalting cells toward concentrating cells

4

are expressed by the following overall mass transport equation [32].

$$J_S(\text{eqcm}^{-2}\text{s}^{-1}) = \lambda i - \mu (C''-C') = (t_K + t_A - 1) \, i/F - \mu (C''-C') = \eta \, i/F = C''J_V \tag{1}$$

$$J_V(\text{cms}^{-1}) = \phi i + \rho (C'' - C') \tag{2}$$

in which, i (A/cm^2) is current density, t_K and t_A are transport number of a cation-exchange membrane (CEM) and an anion-exchange membrane (AEM) respectively, η is current efficiency, λ is the overall transport number, μ is the overall solute permeability, ϕ is the overall electro-osmotic permeability and ρ is the overall volume osmotic permeability.

λ, μ, ϕ are expressed by the following function of ρ.

$$\lambda \ (\text{eq A}^{-1}\text{s}^{-1}) = 9.208 \times 10^{-6} + 1.914 \times 10^{-5} \, \rho \ = (t_K + t_A - 1)/F \tag{3}$$

$$\mu \ (\text{cm s}^{-1}) = 2.005 \times 10^{-4} \, \rho \tag{4}$$

$$\phi \ (\text{cm}^3\text{A}^{-1}\text{s}^{-1}) = 3.768 \times 10^{-3} \, \rho^{\,0.2} - 1.019 \times 10^{-2} \, \rho \tag{5}$$

ρ is presented by the following function of temperature T ($^\circ$C) [33].

$$\rho \ (\text{cm}^4\text{eq}^{-1}\text{s}^{-1}) = 3.421 \times 10^{-3} + 3.333 \times 10^{-4} T \tag{6}$$

The overall membrane pair characteristics λ, μ, ϕ and ρ are determined by setting temperature T ($^\circ$C) using Eqs. (3) – (6).

Eqs. (3) – (6) are introduced for seawater ED incorporating the available properties of the following commercially homogeneous IEMs.

Aciplex CK-2/CA-3, K-172/A172 (Asahi Chemical Co. Japan)

Selemion CVS2/AST, CMR/ASR (Asahi Glass Co., Japan)

Neosepta CL25T/AVS4T, CIMS/ACS3 (Tokuyama Co., Japan)

3.2 Salt concentration and solution velocity in the cells

In Fig. 4, salt concentration in the desalting cells is assumed to be changed linearly from the inlets to the outlets. The average salt concentration C' (eq/cm^3) is expressed by the following equation:

$$C' = (C'_{in} + C'^{*}_{out})/2 \tag{7}$$

$C'_{out}{}^*$ is an unknown parameter at this stage. Superscript * supplied to the unknown parameter denotes the control key.

In the concentrating cells, salt concentration is uniform and it is given from Eqs. (1) and (2) as:

$$C'' = J_S / J_V = \frac{1}{2\rho}\left(\sqrt{A^2 + 4\rho B} - A\right) \tag{8}$$

$$A = \phi i + \mu - \rho C'$$
$$B = \lambda i + \mu C'$$

The average linear velocity u' and u'' (cm/s) in the cells are:

In the desalting cells;

$$u' = (u'_{in} + u'_{out})/2 \tag{9}$$

In the concentrating cells;

$$u'' = (u''_{in} + u''_{out})/2 \tag{10}$$

where u'_{out} and u''_{out} are calculated using the following equations:

$$u'_{out} = u'_{in} - (l/a')J_V \tag{11}$$

$$u''_{out} = u''_{in} + (l/a'')J_V \tag{12}$$

in which, a' and a'' are the flow pass thickness of the desalting cell and concentrating cell, respectively.

C'_{out} and C'' are calculated using the following equations:

$$C'_{out} u'_{out} = C'_{in} u'_{in} - (l/a')J_S \tag{13}$$

$$C'' u''_{out} = C'' u''_{in} + (l/a'')J_S \tag{14}$$

3.3 Decision point 1

C'_{out} calculated above is erroneous because the computation starts by substituting tentatively the determined (unknown) C'^{*}_{out} (control key) in Eq. (7). In order to determine accurate C'_{out}, the following trial-and-error calculation is carried out.

$$C'_{out} = C'^{*}_{out} \tag{15}$$

The calculation loops back and repeats to satisfy Eq. (15).

3.4 Mass transport and electric current

J_S, J_V, η and $t_K + t_A$ are calculated by substituting C' and C'' in Eqs. (1) and (2). Eq. (1) shows that ions in desalting cells are transported to concentrating cells by electro-migration λi and ions move from the concentrating cells to the desalting cells by diffusion $\mu(C'' - C')$. Eq. (2) shows that solutions in desalting cells are transported to concentrating cells by electro-osmosis ϕi and by volume osmosis $\rho(C' - C'')$.

In the electrodialyzer, a part of the electric current does not pass through IEMs and it flows between electrodes through slots and ducts provided in the cells (cf. Fig. 2). i defined in Eqs. (1) and (2) is the effective current density, which does not include the electric current leakage. So, one defines the following effective electric current passing in the electrodialyzer I^{*} (A).

$$I^{*} = iS \tag{16}$$

in which, S (cm^2) is the membrane area. Superscript * denotes the effective electric current as control key.

3.5 Electric resistance of the cells

(1) Electric resistance of a solution in a desalting cell and in a concentrating cell

Diagonal net spacers are incorporated into the desalting cells and concentrating cells. They exert an influence on the electric resistance of both cells. The volume ratio of the spacer in the desalting cell ε' and that of the concentrating cell ε'' are defined by the following equations [30].

$$\varepsilon' = \frac{\pi \, a'}{8 x' \sin\theta'} \tag{17}$$

$$\varepsilon'' = \frac{\pi \, a''}{8 x'' \sin\theta''} \tag{18}$$

7

in which, χ (cm) is the distance between spacer rods and θ (radian) is the crossing angle of the rods (Fig. 3) .

Electric resistance of the desalting cell r' and concentrating cell r'' are given as:

$$r'\left(\Omega\ cm^2\right)=\frac{a'}{\left(1-\varepsilon\ '\right)\kappa\ '} \tag{19}$$

$$r''\left(\Omega\ cm^2\right)=\frac{a''}{\left(1-\varepsilon\ ''\right)\kappa\ ''} \tag{20}$$

Specific conductivity of a salt solution κ in Eqs. (19) and (20) is given by the following function of temperature T (°C) and salt concentration C (g salt/kg solution) [34].

$$\kappa\ (\text{S cm}^{-1}) = (0.9383 + 3.463\times10^{-2}T)\times10^{-3}C - (1.655 + 3.863\times10^{-2}T)\times10^{-6}C^2$$
$$- (1.344 + 3.160\times10^{-2}T)\times10^{-9}C^3 \tag{21}$$

(2) Electric resistance of a membrane pair

Alternating current electric resistance of an IEM pair r_{alter} is expressed by the following function of ρ [35].

$$r_{alter}\ (\Omega\,cm^2) = r_{alter,K} + r_{alter,A} = 1.2323\ \rho^{-(1/3)} \tag{22}$$

in which, $r_{alter,K}$ and $r_{alter,A}$ are alternating electric resistance of a CEM and an AEM. $r_{alter,K} + r_{alter,A}$ is defined as electric resistance of an IEM pair.

Direct current electric resistance of a membrane pair r_{memb} is expressed by the following equation [18].

$$r_{memb}\left(\Omega\ cm^2\right)=\left(\frac{r_{dire}^{\flat}}{r_{alter}}\right)\left(\frac{r_{dire}}{r_{dire}^{\flat}}\right)r_{alter} = r_{dire} \tag{23}$$

$r^{\flat}_{dire}$ in Eq. (23) is measured by passing a direct electric current to a two-cell ED unit supplying low NaCl concentration solutions (specific conductivity κ') to both cells. r_{dire} is measured by passing a direct electric current to above two-cell ED unit supplying a low NaCl concentration solution (specific conductivity κ') to a desalting side (cell) and a high NaCl concentration solution (specific conductivity κ'') to a concentrating side (cell) and subtracting

the effect of membrane potential.

$(r^\flat_{dire}/r_{alter})$ is expressed by the following empirical function of κ'.

$$\log\left(\frac{r^\flat_{dire}}{r_{alter}}\right) = 0.3380 + 0.6386\log\kappa' + 0.2961\left(\log\kappa'\right)^2 \tag{24}$$

$(\kappa_{dire}/r^\flat_{dire})$ is expressed by the following empirical function of κ' and κ''.

$$\frac{r_{dire}}{r^\flat_{dire}} = 1.000 - 0.1359\log\left(\frac{\kappa''}{\kappa'}\right) \tag{25}$$

3.6 Electric Current Leakage

In an electrodialyzer, a part of the electric current does not pass through IEMs and it flows between electrodes through slots and ducts provided in the cells. The structure of the cells is illustrated in Fig. 2. Electric current leakage is an ineffective and inevitable phenomenon which decreases current efficiency and increases substantial energy consumption. Here, one neglects the electric current leakage through direct connections between the cathode and anode by choosing an appropriate length of pipes [36]. As a simplification, one defines the overall electric resistance of the slots r_s (Ω) and the ducts r_d as follows:

$$\frac{1}{r_s} = \frac{1}{r'_s} + \frac{1}{r''_s} = \left(\frac{1}{r'_{s,in}} + \frac{1}{r'_{s,out}}\right) + \left(\frac{1}{r''_{s,in}} + \frac{1}{r''_{s,out}}\right) \tag{26}$$

$$\frac{1}{r_d} = \left(\frac{1}{r'_{d,in}} + \frac{1}{r'_{d,out}}\right) + \left(\frac{1}{r''_{d,in}} + \frac{1}{r''_{d,out}}\right) \tag{27}$$

in which, electric resistance in the slots is given by the following equations:

At the inlets of desalting cells;

$$r'_{s,in} = \frac{h'_s}{\kappa'_{in}\,a'w'n'\left(1-\varepsilon'\right)} \tag{28}$$

At the outlets of desalting cells;

9

$$r'_{s,out} = \frac{h'_s}{\kappa'_{out}\, a'w'n'(1-\varepsilon')} \tag{29}$$

At the inlets of concentrating cells;

$$r''_{s,in} = \frac{h''_s}{\kappa''_{in}\, a''w''n''(1-\varepsilon'')} \tag{30}$$

At the outlets of concentrating cells;

$$r''_{s,out} = \frac{h''_s}{\kappa''_{out}\, a''w''n''(1-\varepsilon'')} \tag{31}$$

In Eqs. (28) – (31), κ is the specific conductance (Eq. (21)) of the solution. h (cm) and w (cm) are the length and width of the slot, respectively. n is number of slots prepared at the head and bottom of a desalting cell. ε is the volume ratio of the spacer (Eqs. (19), (20)).

Electric resistance in ducts is given by the following equations:

At the inlets of desalting cells;

$$r'_{d,in} = \frac{a'+a''+\tau_K+\tau_A}{\kappa'_{in}\, w'h'_d n'} \tag{32}$$

At the outlet of desalting cells;

$$r'_{d,out} = \frac{a'+a''+\tau_K+\tau_A}{\kappa'_{out}\, w'h'_d n'} \tag{33}$$

At the inlets of concentrating cells;

$$r''_{d,in} = \frac{a'+a''+\tau_K+\tau_A}{\kappa''_{in}\, w''h''_d n''} \tag{34}$$

At the outlets of concentrating cells;

$$r''_{d,out} = \frac{a' + a'' + \tau_K + \tau_A}{\kappa''_{out} w'' h''_d n''}$$

(35)

In Eqs. (32) – (35), $a' + a'' + \tau_K + \tau_A$ is the dimension of the duct formed in a cell pair. τ_K and τ_A are the thickness of CEM and AEM, respectively. h (cm) and w (cm) are the length and width of the duct respectively. n is number of ducts prepared at the head and bottom of a desalting cell.

Overall electric resistance in the slots r_s and in the duct r_d are defined in Eqs. (26) and (27). Further, one defines the overall slot electric resistance ratio $r_s^\#$ and the overall duct electric resistance ratio $r_d^\#$ by means of the following equations:

$$r_s^\# = \frac{r_s}{r_{cellpair}}$$

(36)

$$r_d^\# = \frac{r_d}{r_{cellpair}}$$

(37)

$r_{cell\,pair}$ is the following electric resistance per a cell pair.

$$r_{cellpair}\,(\Omega) = (r' + r'' + r_{memb})\frac{1}{S}$$

(38)

Wilson introduced the following leakage current ratio I_L/I by applying the Kirchhoff equation to the equivalent circuit [37].

$$\frac{I_L}{I} = \frac{\displaystyle\sum_{n=1}^{N/2} n^2}{(N/2)\left\{r_s^\# + (1 + r_d^\#)\displaystyle\sum_{n=1}^{N/2} n\right\}} = \frac{2(N+1)(N+2)}{24r_s^\# + 3(1 + r_d^\#)N(N+2)}$$

(39)

3.7 Decision Point 2

The effective electric current I^* passing through the electrodialyzer is decreased due to the electric current leakage I_L. I^* is defined in Eq. (16) and presented as follows.

$$I^* = iS = I - I_L = I\left(1 - \frac{I_L}{I}\right)$$

(40)

I is the electric current supplied from electrodes.

The computer operation in the decision point 2 is: "Adjust the control key I^* to realize Eq. (40)". The calculation loops back and repeats to satisfy all equations described above.

3.8 Cell voltage and energy consumption

Cell voltage V_{cell} is expressed by the following equation.

$$V_{cell}\left(V\,/\,pair\right)=\left(r'+r''+r_{memb}\right)i+2\left(t_K+t_A-1\right)\left(\frac{RT}{F}\right)\ln\left(\frac{\gamma\,''C''}{\gamma\,'C'}\right) \tag{41}$$

γ is the activity coefficient of a component in a solution dissolving strong electrolytes. The component ratio of ions in the solution is assumed to be equivalent to that of seawater. So, γ is expressed by the following function of C (g salt/kg solution) measured for a main component dissolved in seawater; NaCl [38].

$$\gamma = 0.5927 + 0.4355C^{-0.5} - 7.201\times10^{-5}C + 3.503\times10^{-6}C^2 \tag{42}$$

Concentration of electrolytes and NaCl in the concentrated solution (C'' and C''_{NaCl}), NaCl purity of the same solution (p) and the output of electrolytes and NaCl (P and P_{NaCl}) are presented by Eqs. (43) – (47).

$$C''_{NaCl}\,(g/cm^3) = 58.443C''_{Na}\,(eq/cm^3) \tag{43}$$

$$C''(g/cm^3) = 57.87C''(eq/cm^3) \tag{44}$$

$$p = C''_{NaCl}(g/cm^3)/C''(g/cm^3) \tag{45}$$

$$P(t/m^2h) = J_S(t/m^2h) = C''(t/m^3)J_V(m/h) \tag{46}$$

$$P_{NaCl}(t/m^2h) = J_S(t/m^2h)p \tag{47}$$

Energy consumption to produce one ton of total electrolytes E_{total} and NaCl E_{NaCl} is expressed using V_{cell} by the following equations:

$$E_{total}\left(kWh\,/\,tElectrolyte\right) = \frac{V_{cell}\left(I\,/\,S\right)}{P_{total}} \tag{48}$$

$$E_{NaCl}\left(kWh\,/\,tNaCl\right) = \frac{V_{cell}\left(I\,/\,S\right)}{P_{NaCl}} \tag{49}$$

In Eqs. (48) and (49), energy consumption in electrode cells is neglected.

In an ED process using seawater as feed solution, the permeability of divalent ions across the membranes is strongly suppressed for preventing $CaSO_4$ scale precipitation in concentrating cells [39 - 42]. In order to calculate C''_{NaCl} (Eq. (43)) and E_{NaCl} (Eq, (49)), Na^+ ion concentration ratio to total ion concentration in the concentrated solution r_{Na} is given as follows [33].

$$r_{Na}(\text{equiv equiv}^{-1}) = 0.9584 - 4.269 \times 10^{-3}T + (0.7983 + 9.824 \times 10^{-2}T) \times 10^{-2}i^{0.5} \tag{50}$$

Thus the NaCl purity p (Eq. (45)) can be calculated as follows:

$$p = \frac{C''_{NaCl}\left(g\,/\,cm^3\right)}{C''\left(g\,/\,cm^3\right)} = \frac{58.443 r_{Na} C''\left(eq\,/\,cm^3\right)}{57.87 C''\left(eq\,/\,cm^3\right)} = 1.0099 r_{Na} \tag{51}$$

3.9 Pressure drop in the cells and slots

Zimmer and Kotte discussed the relationship between geometry of the diagonal net spacer and the pressure drop [43]. They introduced the hydraulic diameter of the cell incorporated with the spacer. Tsiakis and Papageorgiou applied the hydraulic diameter of the diagonal net spacer to design an ED plant [44]. Based on the above investigations, hydraulic diameter of a desalting cell $d_{H,cell}$ (cm) and a concentrating slot $d_{H,slot}$, incorporated with a diagonal net spacer are expressed by Eqs. (52) and (53).

$$d_{H,cell} = \frac{8 - \pi\,\dfrac{a}{\chi}}{4\left(\dfrac{1}{b} + \dfrac{1}{a}\right) + 2\pi\left(1 - \dfrac{a}{4b}\right)\dfrac{1}{\chi}} \tag{52}$$

$$d_{H,slot} = \frac{8 - \pi \dfrac{a}{\chi}}{4\left(\dfrac{1}{w} + \dfrac{1}{a}\right) + 2\pi \left(1 - \dfrac{a}{4w}\right)\dfrac{1}{\chi}}$$ (53)

in which w is the flow-pass width in the slot (Fig. 2).

Hereafter one does not discriminate the descriptions on the phenomena in the desalting and in the concentrating cells.

The Reynolds number Re of the solution flowing in the cells and slots is less than 3000, so the solution flows in laminar mode. Pressure difference between the inlet and the outlet of the cell (pressure drop in the cell ΔP_{cell}) and that in the slot (pressure drop in the slot ΔP_{slot}) are given by the following Hagen-Poiseuille equation for both desalting and concentrating cells.

$$\Delta P_{cell}(Pa) = \frac{3.2\mu\, l u_{cell}}{\left(d_{H,cell}\right)^2}$$ (54)

$$\Delta P_{slot}(Pa) = \frac{3.2\mu\, h u_{slot}}{\left(d_{H,slot}\right)^2}$$ (55)

in which, l and h are the flow-pass length in the cell and slot (Fig. 2). u_{cell} is the linear velocity in the cell and it is equivalent to u in Eqs. (9) and (10) ($u_{cell} = u$). u_{slot} is the linear velocity in the slot and it is calculated from u_{cell} using the following equation:

$$u_{slot} = \frac{b}{wn}u_{cell}$$ (56)

μ (g cm^{-1}s^{-1}) is the viscosity coefficient of the solution and it is expressed by the following function of temperature T (℃) and salt concentration C (g salt/kg solution) [34].

$$\mu = 1.200\times10^{-2} - 1.224\times10^{-4}T + (2.107\times10^{-5} - 1.529\times10^{-7}T)C + (-1.392\times10^{-8}$$
$$+ 1.123\times10^{-10}T)C^2 + (5.819\times10^{-10} - 6.769\times10^{-12}T)C^3$$ (57)

Head loss ΔH (m) is calculated using:

$$\Delta H_{cell} \text{ (cm)} = 1.01972 \times 10^{-2} \Delta P_{cell}(\text{Pa}) \tag{58}$$

$$\Delta H_{slot} \text{ (cm)} = 1.01972 \times 10^{-2} \Delta P_{slot}(\text{Pa}) \tag{59}$$

Driving power for supplying the solution to a cell pair P_{cell} is:

$$P_{cell}\left(W / pair\right) = \frac{dQ_{cell}\Delta H_{cell}}{6.12\eta_p} \times 10 \tag{60}$$

Q_{cell} is the solution volume rate in a cell;

$$Q_{cell} \text{ (m}^3\text{min}^{-1}) = 60 \times 10^{-6}abu_{cell} \tag{61}$$

Driving power to supply the solution to the slots in a cell pair is calculated by summing up the values at the inlet and the outlet as follows:

$$P_{slot}\left(W / pair\right) = P_{slot,in} + P_{slot,out} = \frac{2dQ_{slot}\Delta H_{slot}}{6.12\eta_p} \times 10 \tag{62}$$

Q_{slot} is the solution volume rate in a slot;

$$Q_{slot} \text{ (m}^3\text{min}^{-1}) = 60 \times 10^{-6}awu_{slot}n \tag{63}$$

η_p is pump efficiency. d is the solution density and it is expressed by the following equation [45].

$$d \text{ (kg/dm}^3) = 1.001 - 1.101 \times 10^{-4}T - 3.356 \times 10^{-6}T^2$$
$$+ (7.881 - 1.368 \times 10^{-2}T + 8.978 \times 10^{-5}T^2) \times 10^{-4}C(\text{g/kg}) \tag{64}$$

In the above equations, the pressure drop in the ducts is neglected.

Driving power due to pressure drops in the cells and slots in a cell pair is:

In the desalting cell;
$$P' \text{ (W/pair)} = P'_{cell} + P'_{slot} \tag{65}$$

15

In the concentrating cell;

$$P''(\text{W/pair}) = P''_{cell} + P''_{slot} \tag{66}$$

Total pump driving power due to pressure drop P_{pump} is defined for a cell pair;

$$P_{pump} (\text{W/pair}) = P' + P'' \tag{67}$$

The ratio of P_{pump} against IV_{cell} is:

$$\frac{P_{pump}}{IV_{cell}} = \frac{P' + P''}{IV_{cell}} \tag{68}$$

3.10 Limiting current density

Limiting current density of an electrodialyzer $(I/S)_{lim}$ is given by the following equation [46].

$$\left(\frac{I}{S}\right)_{lim} = \left\{ l_1 + l_2 \left(\frac{T}{25}\right) + l_3 \left(\frac{T}{25}\right)^2 \right\} \left(m_1 + m_2 u'_{out} \right) \left(C'_{out} \right)^{n_1 + n_2 u'_{out}} \tag{69}$$

where $l_1 = 0.5950$, $l_2 = 0.2731$, $l_3 = 0.1310$, $m_1 = 83.50$, $m_2 = 24.00$, $n_1 = 0.7846$, $n_2 = 8.612 \times 10^{-3}$, T is temperature (℃)

4. Experimental

4.1 Materials and methods: sea water RO discharged brine

RO discharged brine was pumped from the brine deposits of El Prat Sea Water Desalination Waterworks (ITAM-Aigues Ter Llobregat), Barcelona (Spain). Its average composition is shown in Table 1. Various experiments in a range of temperature from 16 to 27℃ and electric current densities from 3.0 to 6.0 A/dm^2 were carried out. The experimental program lasted two years of operation in order to cover the lowest temperature of the Mediterranean Sea in winter time, with temperature up to 10℃ and the highest at summer time up to 28℃. Initial inlet RO discharged brine was oversaturated with calcium carbonate, magnesium carbonate and calcium magnesium carbonate, however, due to the use of anti-scalants on the RO step, scaling problems were not observed. The evolution of the saturation index for NaCl, KCl, MgCl$_2$·6H$_2$O, CaSO$_4$·2H$_2$O, SrSO$_4$, CaCO$_3$, MgCO$_3$ and CaMg(CO$_3$)$_2$ as a function of the IEM-ED concentration process

indicates that the brine could be concentrated up to 4 times (approximately 250 g/l NaCl) without NaCl precipitation risk.

4.2 IEM-ED stack: pilot configuration and operation procedures

The IEM-ED pilot plant has been described elsewhere [19, 20]. The IEM stack was a EURODIA AQUALIZER SV-10 with 50 cell pairs made of Neosepta cation-exchange membranes (CMB) and anion-exchange membranes (AHA) (1000 cm^2 active surface area per membrane). The stack dimensions were 620x450x313 mm. The intermembrane distance was 0.43 mm, whereas linear flow velocity at the inlet of desalting and concentrating cells was around 10.8 cm/s. Photo 1 shows the structure of the cell (U-shape cell). Photo 2 shows the pilot plant.

The brine flow rate through the IEM stack was 0.5 m^3/h in both, the feeding stream and the concentrating stream compartments and 0.15 m^3/h at the electrodes chambers. The feeding and the electrolyte circuits operated in a single-pass design to achieve higher current densities, minimize the problems of the increase of temperature in the cell and the precipitation of calcium sulphate in the feeding compartments. The concentrate stream was re-circulated until the maximum NaCl concentration was reached. Hydrochloric acid was added to keep the pH below 3 for the cathodic circuit, below 7 in the feeding circuit and below 5.5 in the concentrate circuit. Current densities were varied between 3 and 6 A/dm^2. Inlet and outlet temperature were monitored during all the experiments. The RO discharged brine concentration process was monitored by in-line measurements of conductivity, temperature, pH, flow-rate, pressure, current intensity and voltage. Fig. 6 shows the diagram of the main components of the ED pilot plant and monitored parameters.

4.3 Analytical methodologies and chemical analysis

Samples were taken from the concentrate tank, the inlet brine, and the feeding and concentrate flows leaving the stack every 2 hours. Conductivity and temperature of feeding and concentrate streams were monitored during operation to ensure that the concentration process was successful. Sodium chloride, sulphate, calcium and magnesium concentrations in the samples were analyzed. Chloride was determined potentiometrically through precipitation with AgNO$_3$ and a silver chloride electrode (Methrom 721). Calcium and magnesium were determined by Atomic Absorption Spectrophotometry (Perkin Elmer Analyst 300). Sulphate was determined by ionic chromatography (Methrom 761 compact IC equipped with an Anion Dual 2-6.1006.100 column). Finally, sodium chloride was determined by electrically balancing the major ions of the solution.

5. Discussion

Table 2 shows the specifications and operating conditions of the pilot plant electrodialyzer integrated with the imaginary I-shape cells. Pilot plant operation was carried out changing temperature. The computation elucidates the influence of temperature on the plant performance because the program consists of Eqs. (6), (21), (41), (50), (57), (64) and (69) in which temperature T is included. Computation was carried out by inputting the data in Table 2 into the ED program in Fig. 5. Table 3 gives the performance of the ED operation obtained by the experiment (C''_{NaCl}, E_{NaCl}) and the computation (C''_{NaCl}, E_{NaCl}, V_{cell}, α, I_L/I, P_{pump}/IV_{cell}, $(I/S)_{lim}$). The computed data show that the current leakage I_L/L is nearly three percent, the pump driving force P_{pump}/IV_{cell} is ca. $1 - 2$ percent and the limiting current density $(I/S)_{lim}$ is very high (over ten times of current density). However, the desalting ratio α is extremely low, thus the salt concentration at the outlets of desalting cells does not decrease sufficiently. C''_{NaCl} and E_{NaCl} obtained by the experiment are plotted against the computed data and are shown in Figs. 7 and 8, respectively. The correlation coefficients are $R(r) = 0.553$ for C''_{NaCl} (Fig. 7) and $R(r) = 0.863$ for E_{NaCl} (Fig. 8). These figures show that the experimental data are equivalent to the computed data and demonstrate the reasonability of the program.

In order to increase the desalting ratio α in Table 3, the computation was carried out with decreasing the linear velocity at the inlets of desalting cells u'_{in} and concentrating cells u''_{in} from $u'_{in} = u''_{in} = 10.8$ cm/s to 1.0 cm/s keeping $I/S = 4.0$ A/dm^2 and $T = 25$℃ (Table 4). Table 4 shows that α is increased from 0.046 (10.8/s) to 0.61 (1.0 cm/s), however, C''_{NaCl} is decreased and E_{NaCl} is increased with the decrease of the linear velocity. Changes in Table 4 are explained in Fig. 9. Salt concentration of RO discharged brine in this investigation is 69.36 g/dm^3 and it is twice the concentration of seawater. Thus it is necessary to operate the electrodialyzer keeping $\alpha = 0.5$ to reduce salt concentration of a desalted solution to seawater level. In Fig. 9, $\alpha = 0.5$ is realized by keeping the linear velocity $u = 1.18$ cm/s at $I/S = 4.0$ A/dm^2 and $T = 25$℃. However, in this operating condition C''_{NaCl} is decreased to 197.3 g/dm^3 and E_{NaCl} is increased to 186.4 kWh/tNaCl.

In Fig. 10, Line A (Mark ○) shows C''_{NaCl} vs. E_{NaCl} (Table 4, Fig. 9) computed inputting $I/S = 4$ A/dm^2, $T = 25$℃ and $u'_{in} = u''_{in} = 1 - 10.8$ cm/s. Line B (Mark △) is computed inputting $I/S = 2 - 6$ A/dm^2, $T = 25$℃ and $u'_{in} = u''_{in} = 10.8$ cm/s. Line C (Mark □) is computed inputting $I/S = 2 - 6$ A/dm^2, $T = 25$℃ and $\alpha = 0.5$.

Mark ▲ is the data of the pilot plant (EURODIA AQUALIZER) operation obtained in this investigation (Section 4 Experimental) and they are introduced from Table 3. Mark ■ shows data by months reported from the salt manufacturing plant operation to produce edible salt in Japan [47]. The plant specifications and operating conditions are; number of electrodialyzers: 17, total cell pair number: 30,000 pairs, total membrane area: 54,621 m^{2,} average current density:

2.66 A/dm^2, average temperature: 23.5 ℃ (T = 16.0 – 28.2℃).

The Target displayed in the figure (C''_{NaCl} > 200 NaCl g/dm^3, E_{NaCl} < 120 kWh/t NaCl) is the situation to occupy a competitive position in the salt market for industrial use [48].

In Fig. 10, the pilot plant is operated at T = 16 - 27℃; Mark ▲, which is comparable to the Line B (Mark △, T = 25℃). The pilot plant should be operated at lower linear velocity u'_{in} to keep α = 0.5 (Line C, Mark □). u'_{in} at α = 0.5 is plotted against I/S and shown in Fig. 11. The pilot plant should be operated according to Fig. 11 taking into account the effect of temperature on α. However, this operation induces the receding of the plots from the target (C''_{NaCl} is decreased and E_{NaCl} is increased).

The data of the pilot plant operation (Mark ▲) fluctuate largely due to temperature changes and experimental errors. These fluctuations are due to long time pilot plant operations over a period of two years. However, they must be plotted on Line B using the algorithm of the computation if the temperature is adjusted to 25℃ and the experimental errors are removed. Further it should be noted that Line B is nearer to the Target compared to the data of salt manufacturing plant (Mark ■) to produce edible salt. Such an advantage of the pilot plant operation is also recognized if the operation is done keeping α = 0.5 (Line C, Mark □). Thus NaCl produced in the RO discharged brine ED is assumed to be sufficiently competitive in the edible salt market.

Fig. 12 shows the target of this investigation to establish the zero discharge seawater utilization process. By keeping α = 0.5 in ED and returning the desalted solution from ED to RO, water recovery of RO is increased. The product of this process is: drinking water from RO, edible salt and bittern (byproduct) from evaporation (EV), and Cl$_2$, H$_2$ and NaOH from electrolysis (EL). H$_2$ is supplied to fuel cells to generate electric power which is supplied to EL [49]. In order to establish this process, it is necessary to advance ED technology further to increase NaCl concentration and decrease energy consumption.

6. Conclusions

Computer simulation program is fundamentally applied to discuss the performance of an electrodialyzer incorporated with I-shape cells. In this investigation, the program is developed as it is applicable to U-shape cells by assuming the imaginary I-shape cells. The program is applied to compute not only general performance of an electrodialyzer such as mass transport and energy consumption but also specific features such as electric current leakage and pressure drop.

The computed energy consumption and salt concentration of the concentrate are equivalent to the data obtained from the ED pilot plant operation, thus the reasonability of the program is confirmed. The differences between the computed values and experimental values are due to

fluctuations of experimental conditions such as temperature etc. These sources of errors must be taken into account in the next investigation. In order to reduce salt concentration to seawater level for environmental conservation, it is necessary to decrease linear velocity at the inlets of desalting cells and keep the desalting ratio in 0.5. This operating technique decreases salt concentration of concentrated solutions and increases energy consumption. In spite of this operating circumstance, NaCl produced from the RO discharged brine by means of ED is competitive in the edible salt market. However, in order to produce NaCl for industrial use, it is necessary to advance ED technology further to increase NaCl concentration and decrease energy consumption.

REFERENCES

[1] N. Voutchkov, Overview of seawater concentrate disposal alternatives, *Desalination* **273** (2011) 205-219.

[2] MEDRC, Assessment of the Composition of Desalination Plant disposal Brine (Project NO. 98-AS-0.26), Middle East Desalination Research Center (MEDRC), Oman, 2002.

[3] H. Khordagui, Environmental impacts of power-desalination on the gulf marine ecosystem, In: Khan et al. (Eds.), The gulf Ecosystem: Health and Sustainability, Backhuys Publishers, Leiden, 2002.

[4] UNEP/MEDPOL: Sea Water Desalination in the Mediterranean: Assessment and Guidelines, MAP Technical Report Series No. 139, United Nations Environmental Program (UNEP), Mediterranean Action Plan (MAP), Program for the Assessment and Control of Pollution in the Mediterranean region (MEDPOL), Athens, Greece, 2003.

[5] AMBAG, Desalination Feasibility Study in the Monterey Bay Region, prepared for the

Association of Monterey Bay Area Governments (AMBAG), 2006. http://ambag.org/

[6] S. Lattermann, T. Hopner, Environmental impact and impact assessment of seawater desalination, *Desalination* **220** (2008) 1-15.

[7] E. Gacia, O. Invers, M. Manzanera, E. Ballesteros, J. Romero, Impact of the brine from a desalination plant on shallow seagrass (Posidonia Oceanica) meadow, Estuarine, *Coastal and Shelf Science* **72** (2007) 579-590.

[8] R. Danoun. Desalination Plants, Potential Impacts of Brine Discharge on Marine Life, The Ocean Technology Group., University of Sydney, Australia, 2007.

[9] M. Latorre, Congreso Iberico de Gestion y Planificacion del Agua, Costes Economicos y Medio Ambientals de la Desalacion de Aqua de Mar, Tortosa, 2004.

[10] H. Qdais, Environmental impacts of the mega desalination project: The Red Dead Sea conveyor, *Desalination* **220** (2008) 16-23.

[11] R. Kempton, D. Maccioni, S. M. Mrayed, G. Leslie, Thermo dynamic efficiencies and GHG emissions of alternative desalination process, Water Science and Technology: *Water Supply* **10** (2010) 416-427.

[12] A. Pérez-González, A. M. Urtiaga, R. Ibáñez, I. Ortiz, State of the art and review on the treatment technologies of water reverse osmosis concentrates, *Water Research* **46** (2012) 267-283.

[13] P. Xu, T. Y. Cath, A. P. Robertson, M. Reinhard, J. O. Leckie, J. E. Drewes, Critical review of desalination concentrate management, treatment and beneficial use, *Environmental Eng. Sci.* **30** (2013) 502-514.

[14] A. D. Thomas, Zero Discharge Seawater Desalination: Integrating the Production of Freshwater, Salt, Magnesium, and Bromine, Desalination and Water Purification Research and Development Program Report No. 111, Agreement No. 98-FC-81-0054, U. S. Department of the Interior, Bureau of Reclamation, May, 2006.

[15] Y. Zhang, K. Ghyselbrecht, B. Meesschaert, L. Pinoy, B. Van der Bruggen, Electrodialysis on RO concentrate to improve water recovery in wastewater reclamation, *J. Membr. Sci.* **378** (2011) 101-110.

[16] A. T. K. Tran, Y. Zhang, N. Jullok, B. Messchaert, L. Pinoy, B. Van der Bruggen, RO concentrate treatment by a hybrid system consisting of a pellet reactor and electrodialysis, *Chem. Eng. Sci.* **79** (2012) 228-238.

[17] R. K. McGoven, S. M. Zubair, J. H. Lenhard V, The benefits of hybridizing electrodialysis with reverse osmosis, *J. Membr. Sci.* **469** (2014) 326-335.

[18] Y. Tanaka, R. Ehara, S. Itoi, T. Goto, Ion-exchange membrane electrodialytic salt production using brine discharged from a reverse osmosis seawater desalination plant, *J. Membr. Sci.* **222** (2003) 71-86.

[19] S. Casas, N. Bonet, C. Aladjem, J. L. Cortina, E. Larrotcha, L. V. Cremades, Modelling sodium chloride concentration from seawater reverse osmosis brine by electrodialysis: Preliminary results, *Solvent Extraction and Ion Exchange* **29** (2011) 488-508.

[20] M. Reig, S. Casas, C. Aladjem, C. Valderrama, O. Gibert, F. Valero, C. M. Centeno, E. Larrotcha, J. L. Cortina, Concentration of NaCl from seawater reverse osmosis brines for the chlor-alkali industry by electrodialysis, *Desalination* **342** (2014) 107-117.

[21] C. Jiang, Y. Wang, Z. Zhang, T. Xu, Electrodialysis of concentrated brine from RO plant to produce coarse salt and freshwater, *J. Membr. Sci.* **450** (2014) 323-330.

[22] G. Belfort, J. A. Daly, Optimization of an electrodialysis plant, *Desalination* **8** (1970) 153-166.

[23] M. Avriel, N. Zelighter, A computer method for engineering and economic evaluation of electrodialysis plant, *Desalination* **10** (1972) 113-146.

[24] H. J. Lee, F. Sarfert, H. Strathmann, S. H. Moon, Designing of an electrodialysis desalination plant, *Desalination* **142** (2002) 267-286.

[25] P. Moon, G. Sandi, D. Stevens, R. Kizilel, Computational modeling of ionic transport in continuous and batch electrodialysis, *Sep. Sci. Technol.* **29** (2004) 2531-2555.

[26] M. Fidaleo, M. Moresi, Optimal strategy to model the electrodialytic recovery of a strong electrolyte, *J. Membr. Sci.* **260** (2005) 90-111.

[27] M. Sadrzadeh, A. Kaviani, T. Mohammadi, Mathematical modeling of desalination by electrodialysis, *Desalination* **206** (2007) 534-549.

[28] V. V. Nikonenko, N. D. Pismenskaya, A. G. Itoshin, V. I. Zabolotsky, A. A. Shudrenko, Description of mass transfer characteristics of ED and EDI apparatus by using the similarity theory and computation method, Chem. Eng. Process 47 (2008) 1118-1127.

[29] E. Brauns, W. De Wide, B. Van den Bosch, P. Lens, L. Pinoy, M. Empsten, On the experimental verification of an electrodialysis simulation model for optimal stack configuration design through solver software, *Desalination* **24**9 (2009) 1030-1038.

[30] Y. Tanaka, Ion-exchange membrane electrodialysis program and its application to multi-stage continuous saline water desalination, *Desalination* **301** (2012) 10-25.

[31] Y. Tanaka, Ion Exchange Membranes, 2nd edition: Fundamentals and Applications, Elsevier, Amsterdam (2015). http://booksite.elsevier.com/978044463319/

[32] Y. Tanaka, Irreversible thermodynamics and overall mass transport equation in ion-exchange membrane electrodialysis, *J. Membr. Sci.* **281** (2006) 517-531.

[33] Y. Tanaka, Ion-exchange membrane electrodialysis for saline water desalination and application to seawater concentration, *Ind. Eng. Chem. Res.* **50** (2011) 7494-7503.

[34] M. Akiyama, Y. Tanaka, Sea Water Science Research Laboratory, Technical Report, No. 3-22, p. 13, Japan Tobacco & Salt Public Corp. (1992).

[35] Y. Tanaka, Ion-exchange membrane electrodialysis of saline water and its numerical analysis, *Ind. Eng. Chem. Res.* **50** (2011)10765-10777.

[36] R. Yamane, M. Ichikawa, Y. Mizutani, Y. Onoue, Concentrated brine production from sea water by electrodialysis using ion exchange membranes, *Ind. Eng. Chem. Process Des. Dev.* **8** (1969) 159-165.

[37] J. R. Wilson, Demineralization by Electrodialysis, Buther-worth Scientific Publication, London, pp. 265-274 (1969).

[38] H. S. Harned, B. B. Owen, Physical Chemistry of Electrolyte Solutions, p. 726, Reinhold (1998).

[39] Y. Mizutani, R. Yamane, T. Sata, T. Izuo, Permselectivity treatment of a cation-exchange membrane, JP S46-42083 (1971).

[40] K. Mihara, T. Misumi, H. Yamauchi, Y. Ishida, Production of a cation-exchange membrane having excellent specific permeability between cations, JP S47-3081 (1972).

[41] H. Hani, H. Nishimura, Y. Oda, Anion-exchange membrane having permselectivity between anions, JP S36-15258 (1961).

[42] K. Mihara, T. Misuni, H. Yamauchi, Y. Ishida, Anion-exchange membrane having excellent specific permeability between anions, JP S45-19980, S45-30693 (1970).

[43] C. C. Zimmer, V. Kotte, Effects of spacer geometry on pressure drop, mass transfer, mixing behavior, and residence time distribution, *Desalination* **104** (1996) 129-134.

[44] P. Tsiakis, L. G. Papageorgiou, Optimum design of an electrodialysis brackish water desalination plant, *Desalination* **173** (2005) 173-186.

[45] K. Sato, T. Matsuo, Seawater Handbook, Soc. Sea Water Sci. Jpn., p. 10 (1974).

[46] Y. Tanaka, Mass transport in ion-exchange membranes, In: Encyclopedia of Membrane Science and Technology (Eds. M. V. Hoek, V. V. Tarabara), John Wiley & Sons, Inc. (2013).

[47] Salt manufacturing plant technical report, Salt Industry Center, Jpn. (1998).

[48] T. Fujita, Current challenges of salt production technology, *Bull. Soc. Sea Water Sci. Jpn.* **63** (2009) 15-20.

[49] S. Bebelis, K. Bouzek, A. Cornell, M. G. S. Ferreira, G. H. Kelsall, F. Lapique, C. Ponce de Leon, M. A. Rodrigo, F. C. Walsh, Highlight during the development of electrochemical engineering, *Chem. Eng. Res. Des.* **91** (2013) 1998-2020.
http://www.cleanenergyactionproject.com

NOMENCLATURES

a flow-pass thickness in a desalting and a concentrating cell (cm)

b flow-pass width in a desalting and a concentrating cell (cm)

C electrolyte concentration (eq cm^{-3}, eq dm^{-3}, g dm^{-3})

d solution density

d_H hydraulic diameter (cm)

E energy consumption (kWh t^{-1})

F Faraday constant (As eq^{-1})

h length of a slot and a duct (cm)

i effective current density (Acm^{-2}, Adm^{-2})

I total electric current (A)

I^* effective electric current (A)

I_L electric current leakage (A)

I/S average current density (Acm^{-2}, Adm^{-2})

$(I/S)_{\lim}$ limiting current density (Acm^{-2})

J_S ion flux across a membrane pair (eq cm^{-2}s^{-1}), (t m^{-2}h^{-1})

J_V solution flux across a membrane pair (cm s^{-1}), (m h^{-1})

l flow-pass length in a desalting and a concentrating cell (cm)

n number of slots in a cell

N number of cell pairs in a stack

p NaCl purity in a concentrate (g/g)

P output (t m^{-2}h^{-1}); driving power (W/pair)

P_{pump} pump driving power (W/pair)

Q solution volume rate (m^{3}min^{-1})

r electric resistance (Ω cm^2)

r_{alter} altering current electric resistance (Ω cm^2)

$r_{cellpair}$ electric resistance of a cell pair (Ω cm^2)

r_{dire} direct current electric resistance (Ω cm^2)

r_{memb} direct current electric resistance of a membrane pair (Ω cm^2)

r_{Na} Na$^+$ ion concentration ratio in concentrate (eqv./eqv.)

R gas constant (JK^{-1}mol^{-1})

S ion-exchange membrane area (cm^2)

t transport number of ions in a membrane

T temperature (℃, K)

u linear velocity in desalting and concentrating cells (cm s^{-1})

V_{cell} cell voltage (V pair^{-1})

V_{memb} membrane potential (V pair^{-1})

V_{Ω} Ohmic potential (V pair^{-1})

w width of a slot and a duct (cm)


Greek letters

α desalting ratio

γ activity coefficient of electrolytes in a solution

ΔH head loss (m)

ΔP pressure drop (Pa)

ε volume ratio of a spacer in a desalting and a concentrating cell

η current efficiency

η_p pump efficiency

κ specific conductivity of a solution (mS cm^{-1})

θ crossing angle of spacer rods (radian)

λ overall transport number of a membrane pair (eq A^{-1}s^{-1})

μ overall solute permeability of a membrane pair (cm s^{-1}); viscosity coefficient (g cm^{-1}s^{-1})

ρ overall volume osmotic permeability of a membrane pair (cm^{4}eq^{-1}s^{-1})

τ thickness of an ion-exchange membrane (cm)

ϕ overall electro-osmotic permeability of a membrane pair (cm^{3}A^{-1}s^{-1})

χ distance between spacer rods (cm)

Subscripts

A   anion-exchange membrane

cell   cell

d   duct

in   inlet

K   cation-exchange membrane

out   outlet

s, slot   slot

Superscripts

'   desalting cell

"   concentrating cell

*   control key

overall
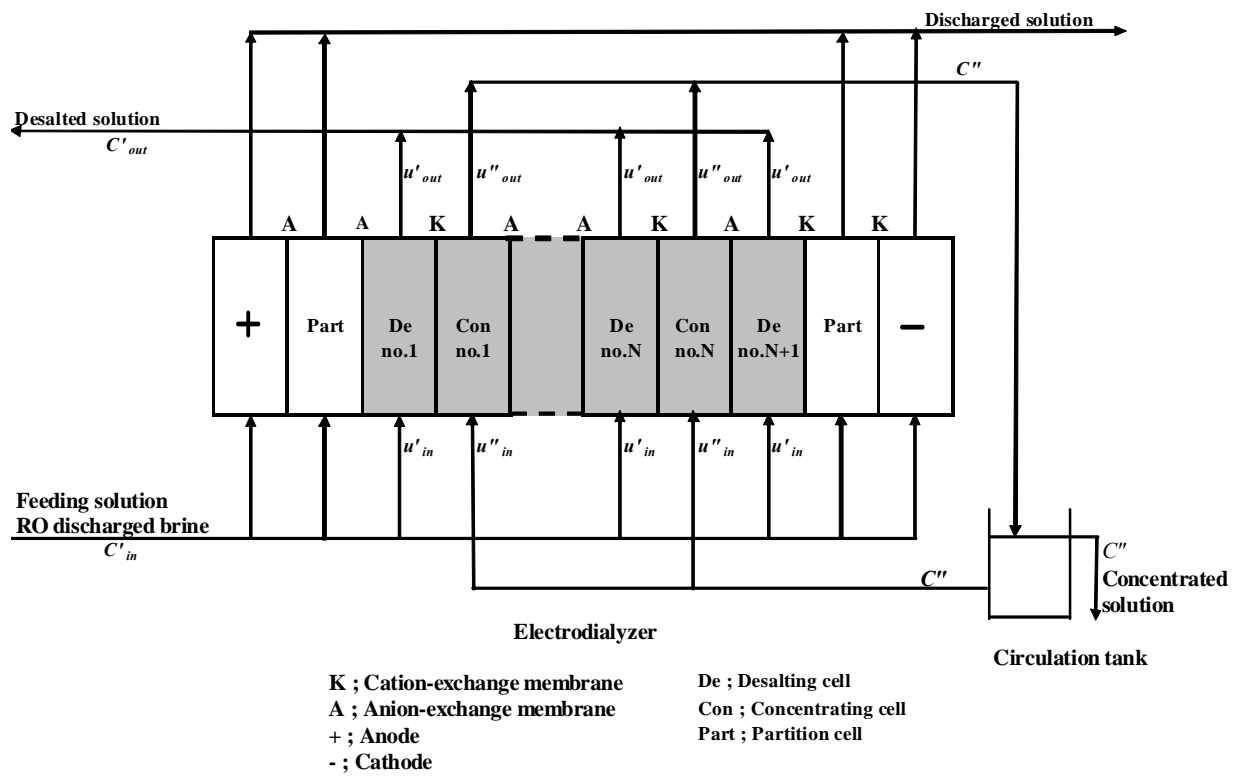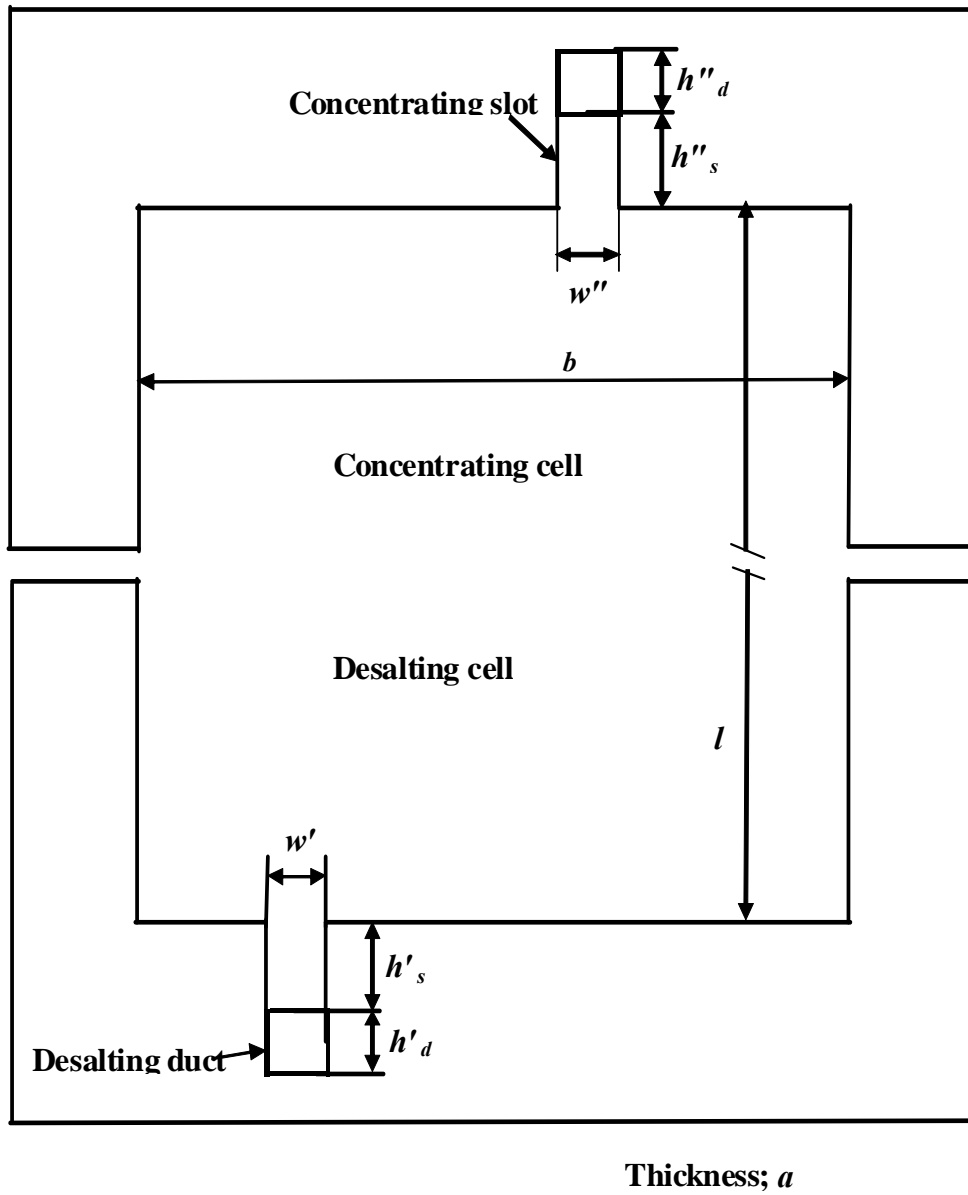
Fig. 1   Electrodialysis process.

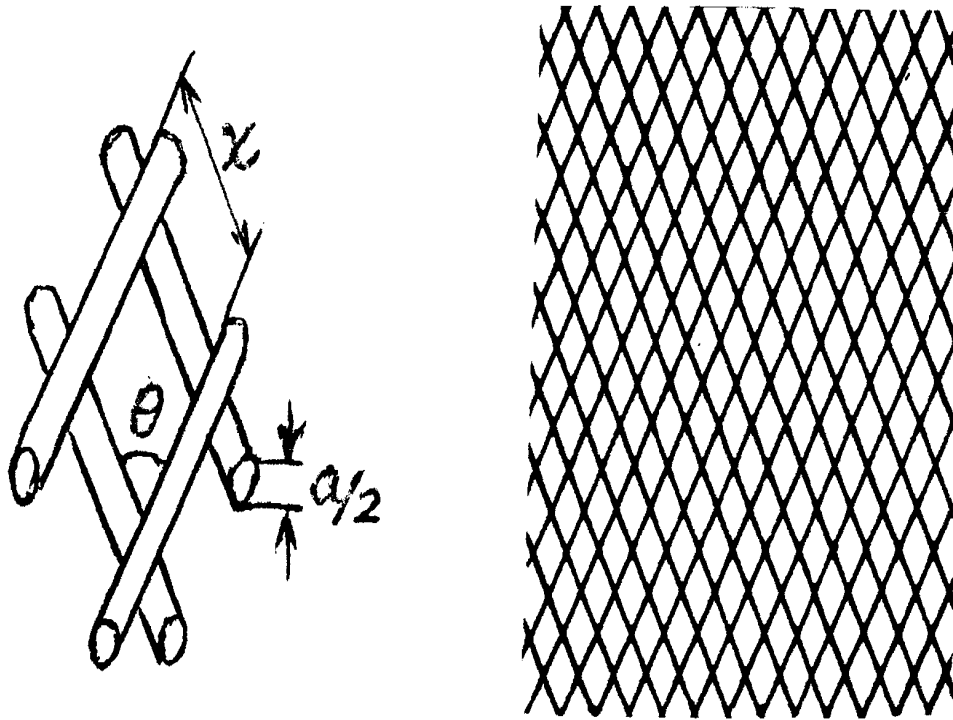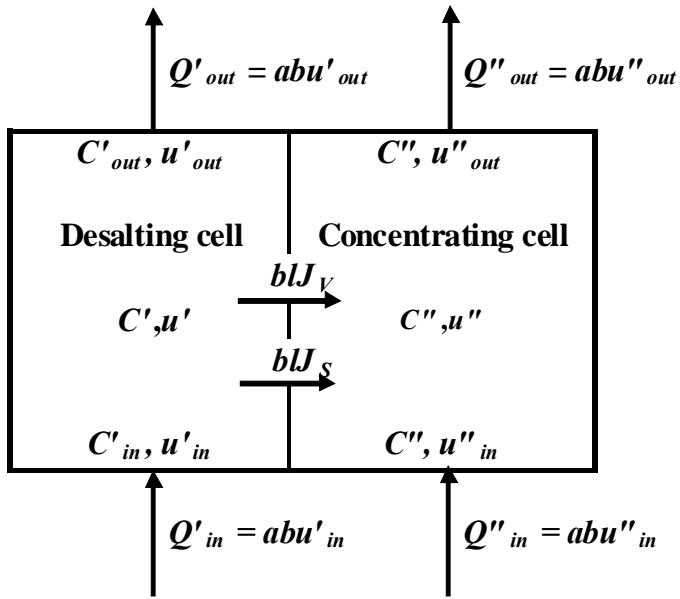**Fig. 2   Structure of a desalting cell and a concentrating cell.**

Fig. 3 Structure of a spacer.

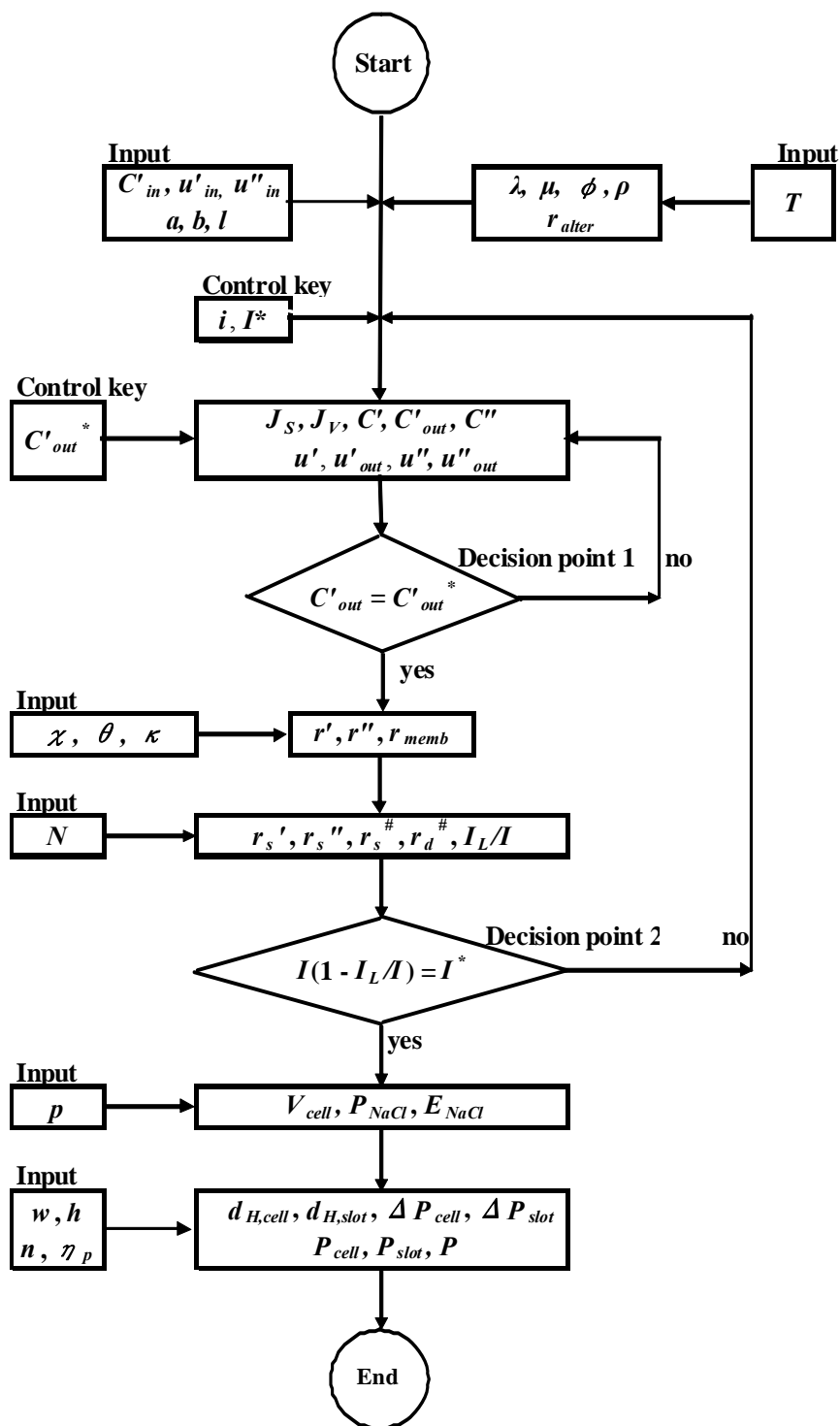**Fig. 4   Mass transport in a desalting cell and a in concentrating cell.**

Start

Input
C'_{in}, u'_{in}, u''_{in}
a, b, l

λ, μ, ϕ, ρ
r_{alter}

Input
T

Control key
i, $I*$

Control key
$C'_{out}{}^*$

J_S, J_V, C', C'_{out}, C''
u', u'_{out}, u'', u''_{out}

Decision point 1   **no**

$C'_{out} = C'_{out}{}^*$

yes

Input
χ, θ, κ

r', r'', r_{memb}

Input
N

$r_s{}'$, $r_s{}''$, $r_s{}^{\#}$, $r_d{}^{\#}$, I_L/I

Decision point 2   **no**

$I(1 - I_L/I) = I^*$

yes

Input
p

V_{cell}, P_{NaCl}, E_{NaCl}

Input
w, h
n, η_p

$d_{H,cell}$, $d_{H,slot}$, ΔP_{cell}, ΔP_{slot}
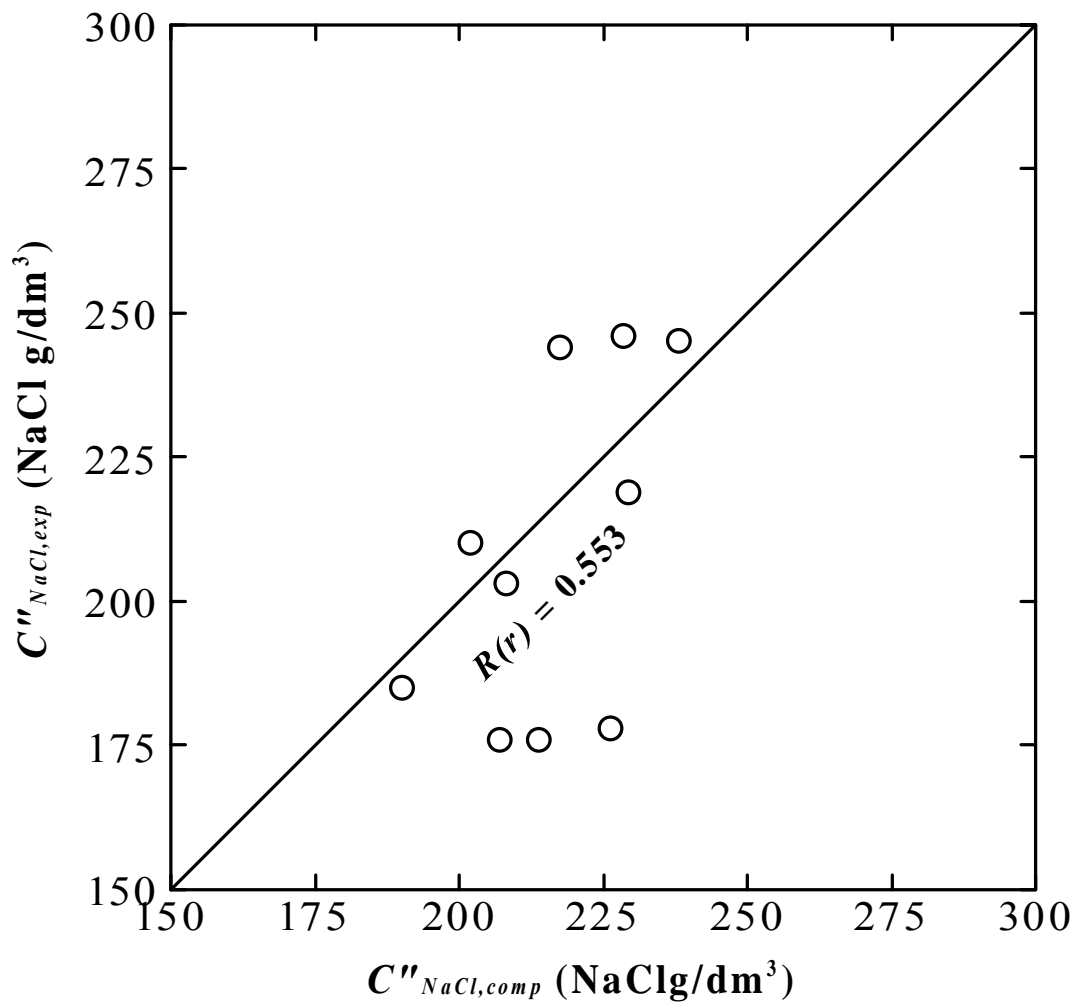P_{cell}, P_{slot}, P

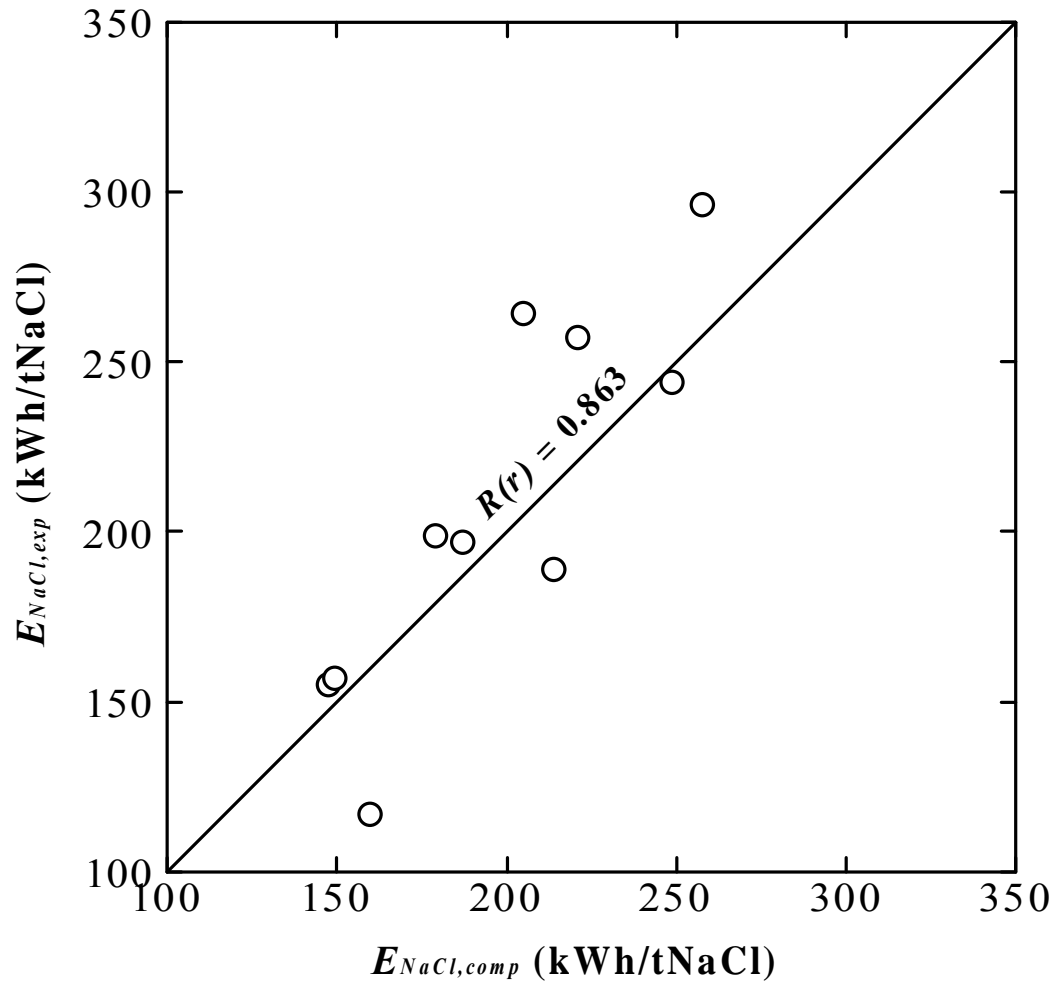**End**

Fig. 5   Electrodialysis program chart.
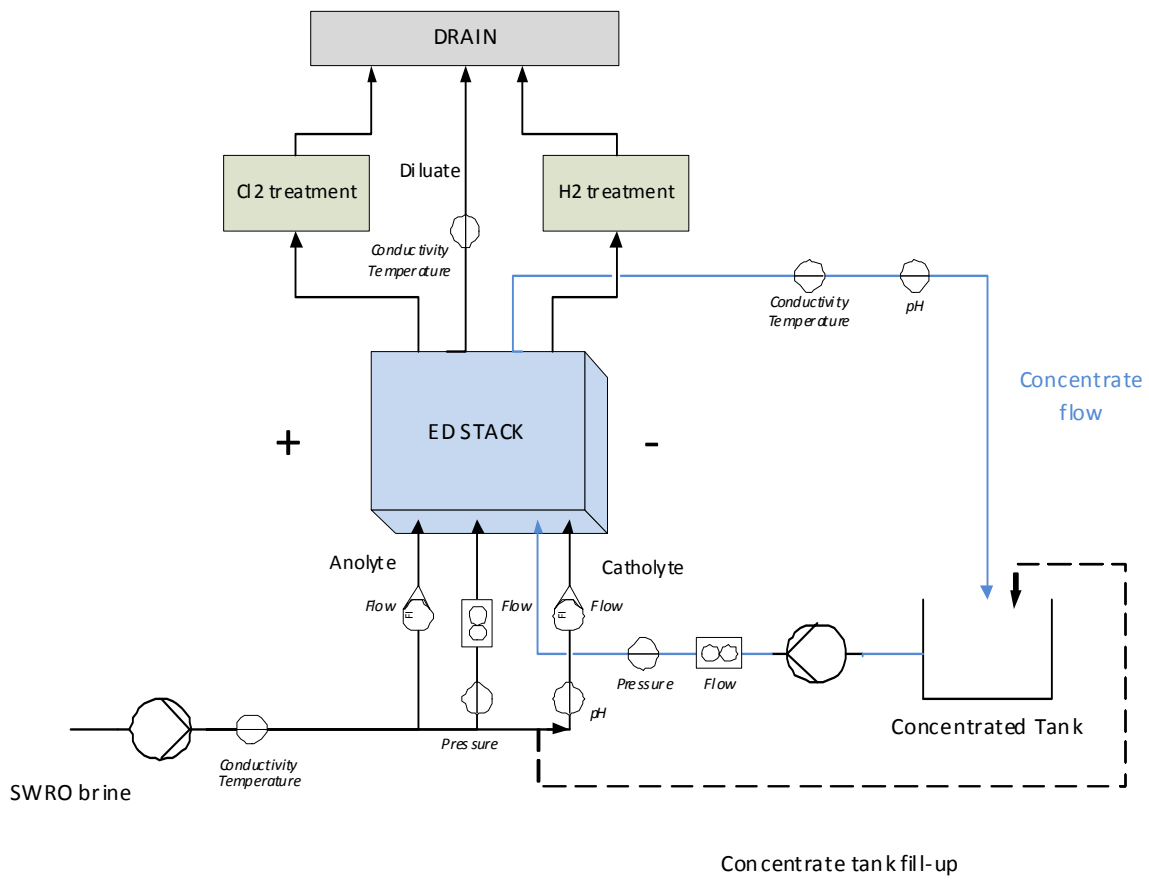
**Fig. 6   Diagram of the main components of the ED pilot plant
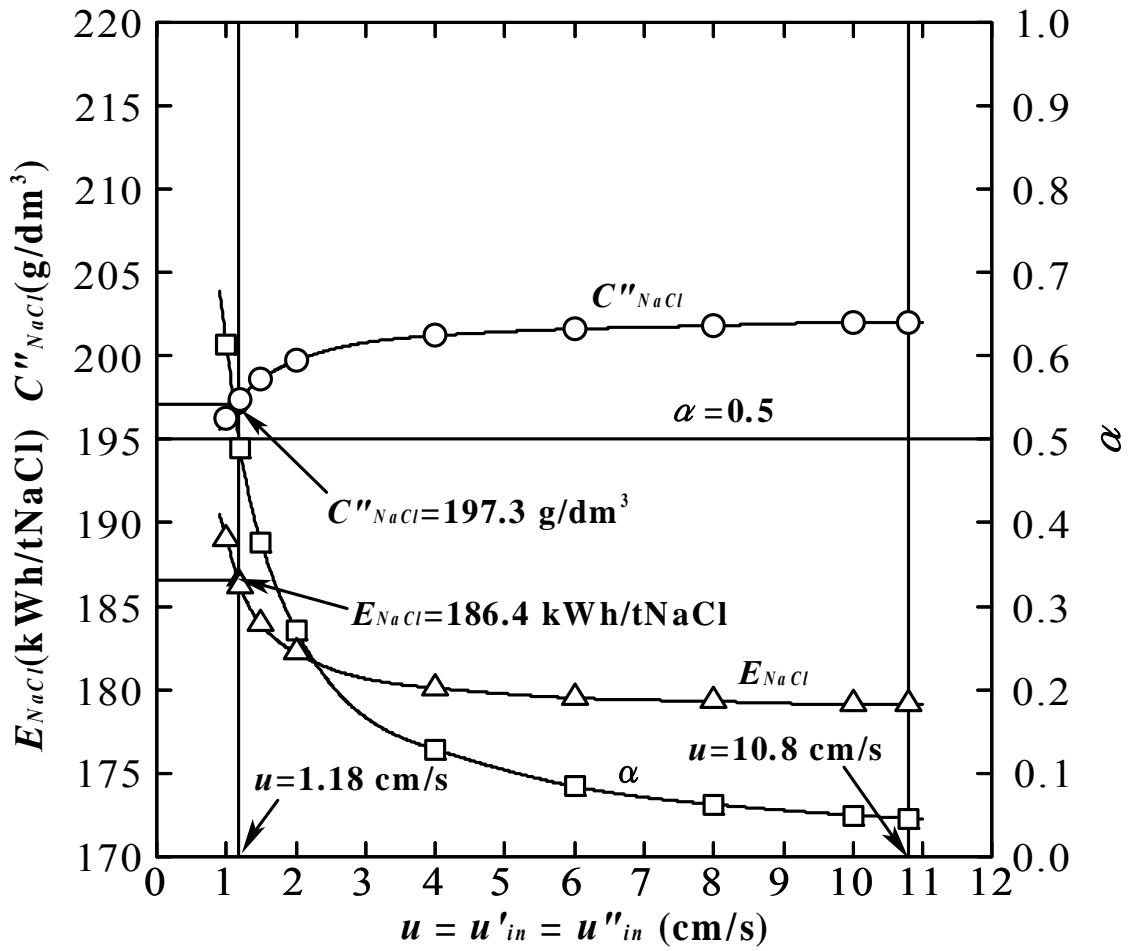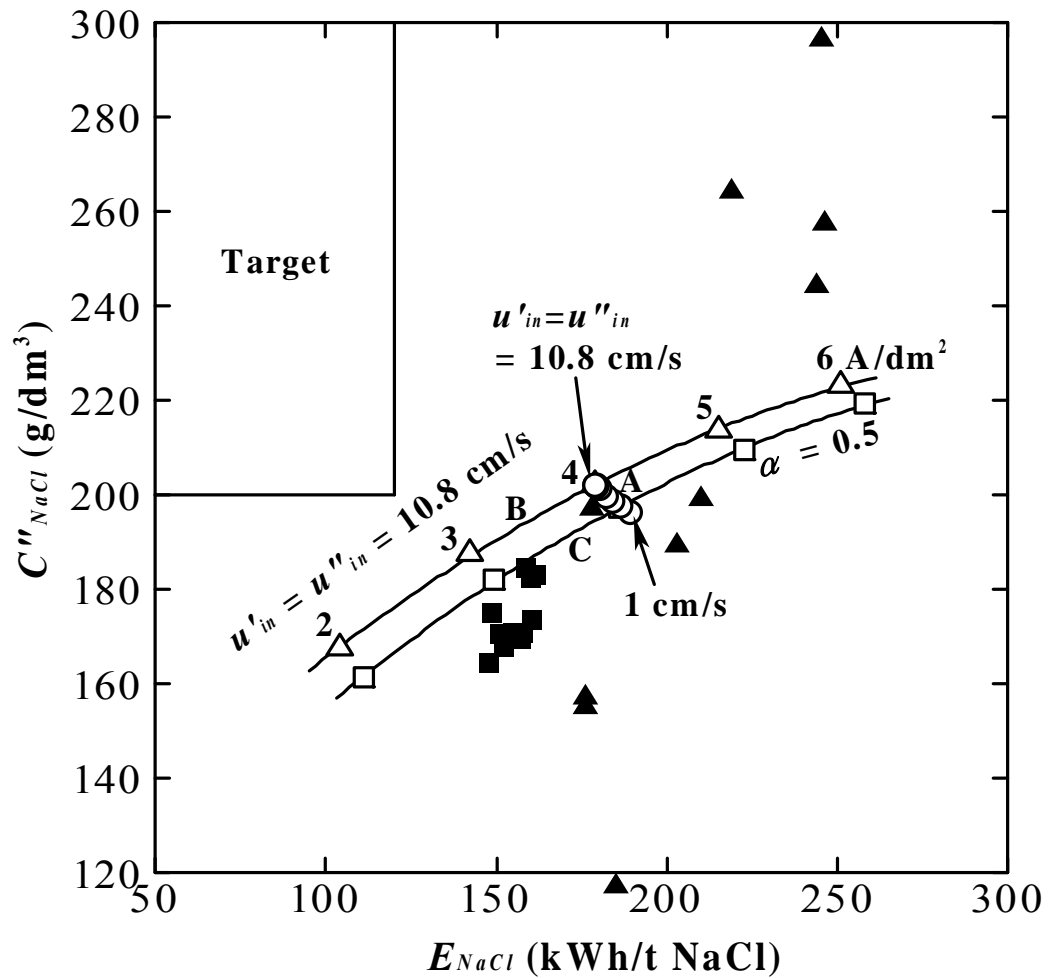and parameters monitored.**

Fig. 7　NaCl concentration in the concentrated solution.

Fig. 8 Energy consumption.

Fig. 9 Influence of linear velocity to NaCl concentration and energy consumption.
$I/S = 4 \, \text{A/dm}^2$, $T = 25℃$

Fig. 10 Relationship between NaCl concentration and energy consumption to produce one ton of NaCl.

Program computation

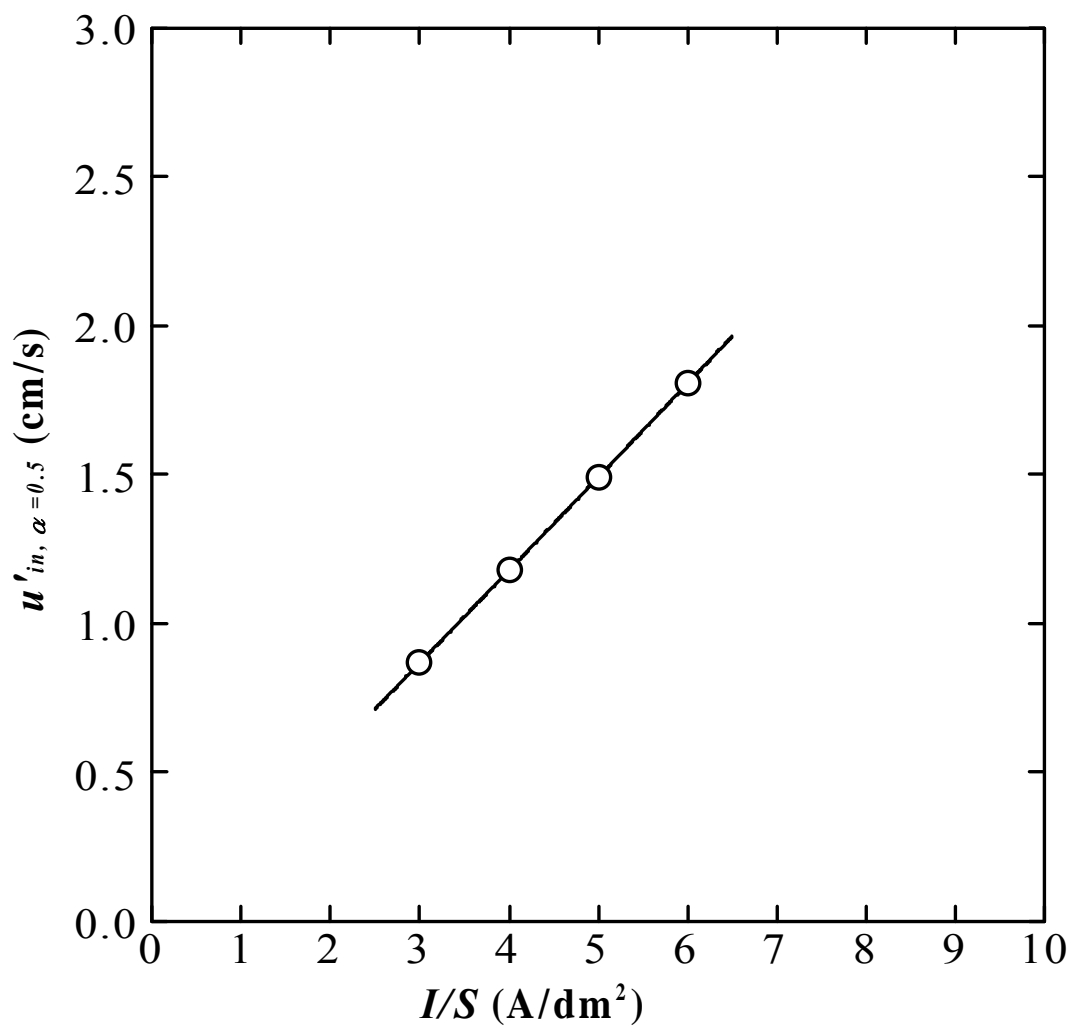○ 4 A/dm^2, 25℃, $u'_{in} = u''_{in} = 1 – 10.8$ cm/s; Line A

△ 2 – 6 A/dm^2, 25℃, $u'_{in} = u''_{in} = 10.8$ cm/s; Line B
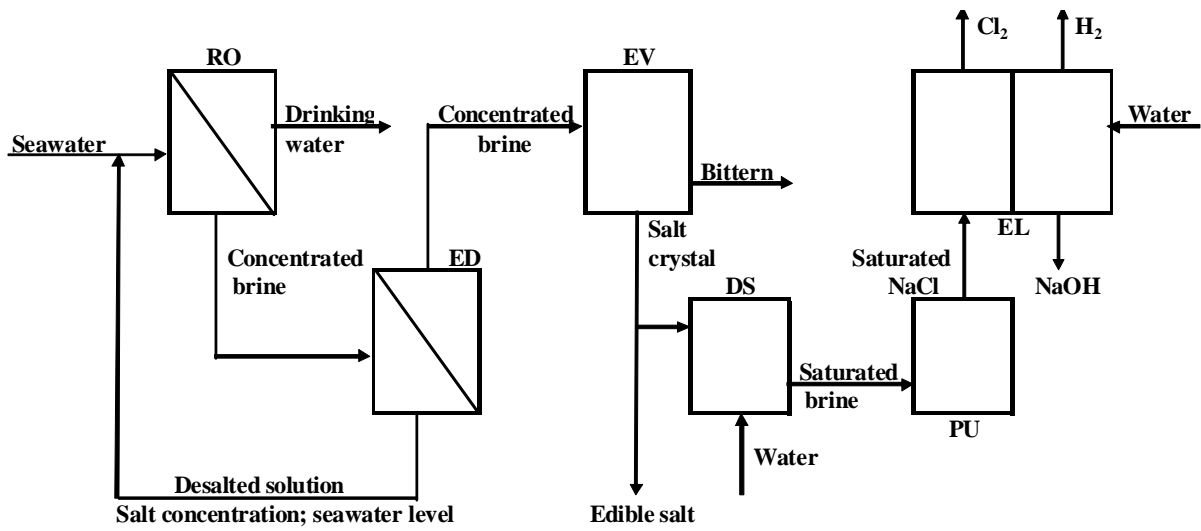
□ 2 – 6 A/dm^2, 25℃, $\alpha = 0.5$; Line C

Plant operation

▲ Pilot plant operation (EURODIA AQUALIZER, Spain)

■ Salt manufacturing plant operation
(Seawater electrodialyzer, Japan)

Fig. 11 Linear velocity at the inlet of desalting cells at desalting ratio $\alpha = 0.5$.
$T = 25°C$

Fig. 12   Zero discharge seawater utilization process

RO; Reverse osmosis   EV; Evaporation   EL; Electrolysis
ED; Electrodialysis   DS; Dissolution   PU; Purification

Table 1 **Average of the RO discharged brine from the ITAM-El Prat Desalination water works (Barcelona, Spain)**

Major components[1]	Concentration (g/L)	Minor components[2]	Concentration (mg/L)
Cl^-	38.8±0.4	Si	< 1
Br^-	0.13±0.06	Al	< 0.5
SO_4^{2-}	5.41±0.2	Fe	< 0.2
Mg^{2+}	2.64±0.2	Ba	< 0.2
Ca^{2+}	0.83±0.04	Ni	0.07±0.02
K^+	0.75±0.05	Cu	0.03±0.01
Na^+	20.8±0.3	Mn	0.01±0.01
Sr^{2+}	0.016±0.003	Cr	0.007±0.003

[1] Concentration values correspond to the ionic forms

[2] Concentration values correspond to the total element concentration

Table 2   Specifications and operating conditions of the pilot plant electrodialyzer integrated with imaginary I-shape cells.

|		
Flow-pass thickness in a desalting and a concentrating cell: $a = a' = a''$	0.043	cm
Flow-pass width in a desalting and a concentrating cell: b	10	cm
Flow-pass length in a desalting and a concentrating cell: l	100	cm
Membrane area: S	1000	cm^2
Thickness of a cation-exchange membrane: τ_K	0.018	cm
Thickness of an anion-exchange membrane: τ_A	0.015	cm
Slot and duct number in a desalting cell: n'	1	
Slot and duct width in a desalting cell: w'	3	cm
Slot and duct length in a desalting cell: h'	2	cm
Slot and duct number in a concentrating cell: n''	1	
Slot and duct width in a concentrating cell: w''	3	cm
Slot and duct length in a concentrating cell: h''	2	cm
Rod distance of a spacer: χ	0.1	cm
Crossing angle of rods of a spacer: θ	$\pi/2$	radian
Number of cell pairs: N	50	pairs
Linear velocity at the inlet of desalting cells: u'_{in}	10.8	cm/s
Linear velocity at the inlet of desalting cells: u''_{in}	10.8	cm/s
Salt concentration at the inlets of desalting cells (RO discharged brine): C'_{in}	69.36	g/dm^3
Current density: I/S	3.0, 3.5, 4.0, 4.5, 5.0, 6.0	A/dm^2
Temperature: T	16 - 27	℃

Table 3   Performance of RO discharged brine electrodialysis: experiments and computations

No.	I/S	T	Experiment		Computation						
			C''_{NaCl}	E_{NaCl}	C''_{NaCl}	E_{NaCl}	V_{cell}	α	I_L/I	P_{pump}/IV_{cell}	$(I/S)_{lim}$
	A/dm²	℃	NaClg/dm³	kWh/NaCl t	NaClg/dm³	kWh/NaCl t	V/pair				A/dm²
1	6.0	27	244	244	217.5	248.8	0.4004	0.07220	0.03482	0.007072	91.04
2	6.0	20	245	296	238.1	257.4	0.4278	0.07358	0.03248	0.007536	78.25
3	5.0	27	203	189	208.2	213.6	0.3428	0.58860	0.03462	0.009655	92.23
4	5.0	20	246	257	228.4	220.7	0.3658	0.06012	0.03237	0.010284	79.29
5	4.5	18	219	264	229.3	204.8	0.3422	0.05384	0.03165	0.012481	76.41
6	4.0	25	210	199	202.0	179.1	0.2892	0.04605	0.03368	0.014372	89.47
7	4.0	17	178	197	226.3	187.2	0.3137	0.04739	0.03124	0.015329	75.26
8	3.5	27	185	117	190.1	159.7	0.2550	0.03929	0.03406	0.017659	93.97
9	3.0	18	176	155	207.1	147.3	0.2449	0.03416	0.03120	0.024645	77.86
10	3.0	16	176	157	213.8	149.5	0.2507	0.03447	0.03064	0.024963	74.57

Table 4   Influence of linear velocity to the performance of RO discharged brine electrodialysis.

I/S = 4.0 A/dm², T = 25 ℃

$u'_{in} = u''_{in}$	C''_{NaCl}	E_{NaCl}	V_{cell}	α	I_L/I	P_{pump}/IV_{cell}	$(I/S)_{lim}$
cm/s	NaClg/dm³	kWh/NaCl t	V/pair				A/dm²
10.8	202.0	179.1	0.2892	0.04605	0.03368	0.014372	89.47
10.0	202.0	179.1	0.2893	0.04980	0.03367	0.012321	88.11
8.0	201.8	179.3	0.2896	0.06257	0.03360	0.007883	83.13
6.0	201.6	179.5	0.2900	0.08414	0.03350	0.004432	75.39
4.0	201.2	180.1	0.2910	0.12841	0.03328	0.001967	63.85
2.0	199.7	182.2	0.2944	0.27118	0.03258	0.000489	45.14
1.5	198.6	183.9	0.2974	0.37578	0.03209	0.000274	37.23
1.2	197.4	186.2	0.3010	0.48921	0.03156	0.000174	30.31
1.0	196.2	189.0	0.3058	0.61284	0.03102	0.000120	23.54
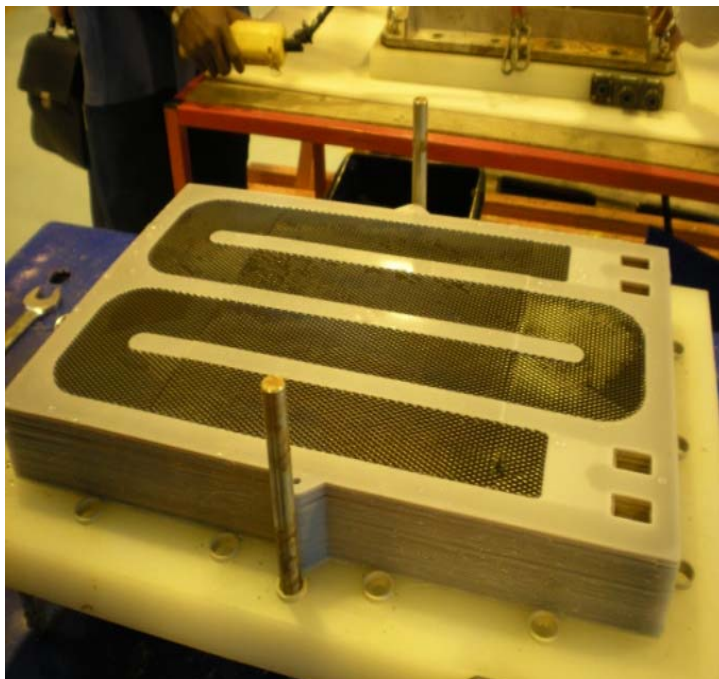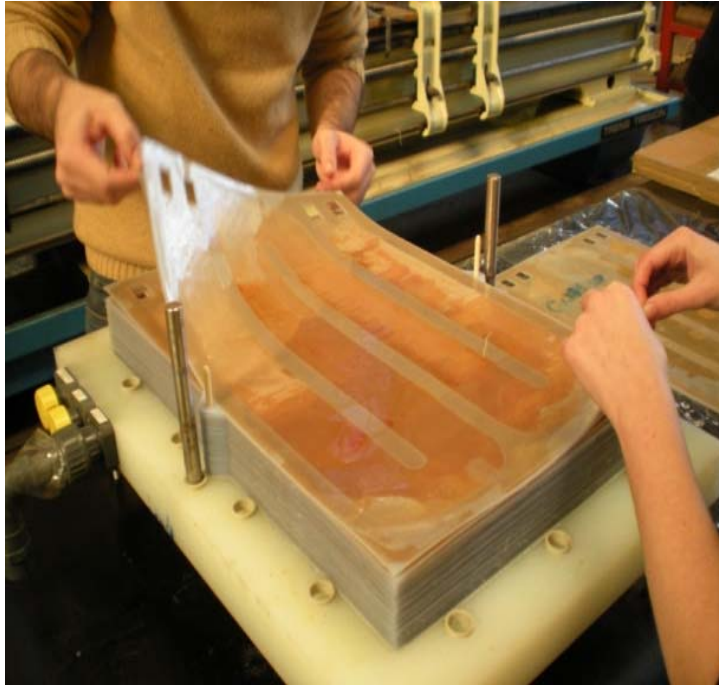
Photo 1   Structure of the U-shape cell

Photo 2   ED pilot plant located at the El Prat Seawater Desalination Plant.